CHINESE OPTICS LETTERS
Vol. 19, No. 10 | October 2021

Donut-like photonic nanojet with reverse energy flow

Hao Wang (王 浩)[1], Jingjing Hao (郝晶晶)[2], Baifu Zhang (张柏富)[1*], Cheng Han (韩 成)[1], Chunguang Zhao (赵春光)[2], Zhe Shen (沈 哲)[1], Ji Xu (许 吉)[3], and Jianping Ding (丁剑平)[4**]

[1] School of Electronic and Optical Engineering, Nanjing University of Science and Technology, Nanjing 210094, China

[2] The 28th Research Institute of China Electronics Technology Group Corporation, Nanjing 210007, China

[3] College of Electronic and Optical Engineering & College of Microelectronics, Nanjing University of Posts and Telecommunications, Nanjing 210023, China

[4] Collaborative Innovation Center of Advanced Microstructures and School of Physics, Nanjing University, Nanjing 210093, China

*Corresponding author: zhangbf@njust.edu.cn

**Corresponding author: jpding@nju.edu.cn

Received February 3, 2021 | Accepted March 18, 2021 | Posted Online August 13, 2021

Photonic nanojets (PNJs) are subwavelength jet-like propagating waves generated by illuminating a dielectric microstructure with an electromagnetic wave, conventionally a linearly polarized plane wave. Here, we study the donut-like PNJ produced when a circularly polarized vortex beam is used instead. This novel PNJ also has a reverse energy flow at the donut-like focal plane depending on both the optical vortex topological charge and microsphere size. Our tunable PNJ, which we investigate numerically and analytically, can find applications in optical micromanipulation and trapping.

Keywords: photonic nanojet; optical vortex; reverse energy flow.

DOI: 10.3788/COL202119.102602

1. Introduction

The photonic nanojet (PNJ), which was first discovered by Chen *et al.* in 2004[1], is a tightly confined light beam that emerges from the shadow side of a wavelength-scale dielectric particle under optical illumination. Because the PNJ has a high-intensity peak and narrow, subwavelength waist, which it maintains for a propagation distance typically longer than a wavelength, it has possible applications in ultramicroscopic technology[2–5], super-resolution optical imaging[6,7], nano-patterning[8,9], optical micromanipulation[10–12], optical data storage[13,14], and other fields.

The formation of a PNJ is a complex process that involves refraction, interference, and diffraction of an electromagnetic wave incident on a dielectric particle at the wavelength scale. By tuning the diameter and refractive index of the illuminated dielectric structure (customarily assumed to be a cylinder or sphere), the properties of the generated PNJ, including the maximum intensity, PNJ length, and full width at half-maximum (FWHM), can be greatly modified[15,16]. Recently, novel PNJs generated by dielectric particles with more complicated geometries have also been proposed and investigated. For example, the two-layer dielectric microsphere[17], liquid-filled hollow microcylinder[18], and microtoroid structures[19] have been designed, which produce ultralong PNJs with propagation lengths of a few tens of wavelengths. By illuminating a dielectric trapezoid particle, bent PNJs known as "photonic hooks" can be formed with modified propagation paths[20–22].

However, while various dielectric structures have been investigated, the incident light source of PNJs in most studies has been restricted to a simple plane wave. If we attribute the generation of a PNJ to a process analogous to the jet-like nanofocusing in the near-field region[23], naturally, the complicated incident light field will affect the focusing properties heavily and can be expected to play a role in structuring of special PNJs[24–26]. Thus, it is of interest to study the dependence of PNJ focusing properties on both the structured polarization state and phase distribution and explore the related novel effects.

In this Letter, we propose and numerically investigate a novel PNJ generated by a circularly polarized vortex beam incident on a dielectric microsphere. The PNJ appears as a donut-like focal field with longitudinal reverse energy flow; such a flow could greatly enhance capabilities in the fields of optical micromanipulation and trapping. The dependence of the reverse energy flow of the donut-like PNJ on both the topological charge of the vortex beam and the geometry of the microsphere is investigated in detail. The unique properties of the PNJ are similar to those associated with vector diffraction of an incident light beam focused by a high numerical aperture (NA) lens, a problem that can be treated analytically using the Richards–Wolf (RW) integral.

2. Results and Discussions

Figure 1 shows schematically a donut-like PNJ generated by a dielectric microsphere with radius R. The incident light

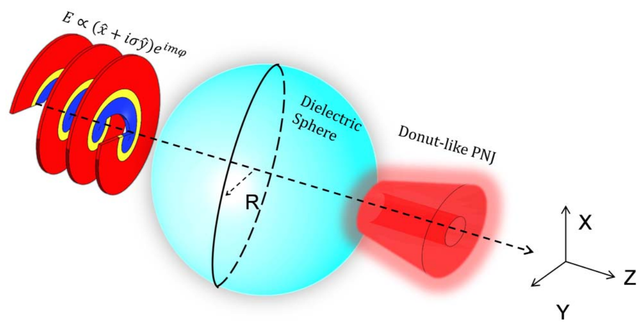

Fig. 1. Schematic of the generation of a donut-like photonic nanojet (PNJ). Incident light has circular polarization σ and topological charge m.

propagating along the z axis is a circularly polarized Laguerre–Gaussian (LG) beam with a vortex phase:

$$E \propto E_0(\hat{x} + i\sigma\hat{y})e^{ikz}\left(\frac{\sqrt{2}r}{\omega_0}\right)^{|m|} e^{(-\frac{r^2}{\omega_0^2})} e^{im\phi}, \tag{1}$$

where E_0 is the amplitude; $\hat{x}$ and $\hat{y}$ are unit vectors; $r = \sqrt{x^2 + y^2}$; $\sigma = \pm 1$ refer to the right circular polarization (RCP) and left circular polarization (LCP), respectively; ω_0 is the Gaussian parameter; k is the wave vector; and m is the topological charge of the optical vortex. The dependence of donut-like PNJ properties on the parameters R and m is numerically studied by three-dimensional (3D) finite-difference time-domain (FDTD) simulations based on Lumerical FDTD software. For simplicity, but without loss of generality, we fix refractive index $n = 1.5$, wavelength $\lambda = 632.8$ nm, and $\sigma = -1$ in this Letter.

The electric field intensity distribution $|E|^2$ of the proposed donut-like PNJ is shown in Fig. 2. When an LCP-LG vortex beam with $m = 2$ is used, the generated PNJ's profile exhibits a hollow-ring focus [Figs. 2(a) and 2(c)]. By contrast, the conventional PNJ generated by Gaussian-beam illumination ($m = 0$) has a classical jet-like focal field [Figs. 2(b) and 2(d)]. The presence in the donut-like PNJ of a subwavelength focusing tube (FWHM $= 0.44\lambda$) beyond the diffraction limit hints at novel applications such as ultracompact optical trapping and micromanipulation.

Another unique property of the proposed donut-like PNJ is the appearance of reverse energy flow along the optical axis in the vicinity of the focal plane. We investigate the PNJ generated by microspheres with radii ranging from 3λ to 7λ and find reverse energy flow in all cases. Figure 3(a) shows that, as the radius of the dielectric microsphere increases, the absolute value of the longitudinal reverse flow P_z rises to its maximum value when $R = 6\lambda$, then shows a diminishing trend. Figure 3(b) plots the longitudinal energy flow of the donut-like PNJ along the x axis in the focal plane as a function of the refractive index of the microsphere. As the refractive index changes, the magnitude of the reverse energy flow varies; it takes its maximum value around $n = 1.5$, indicating that PNJ properties can be tuned

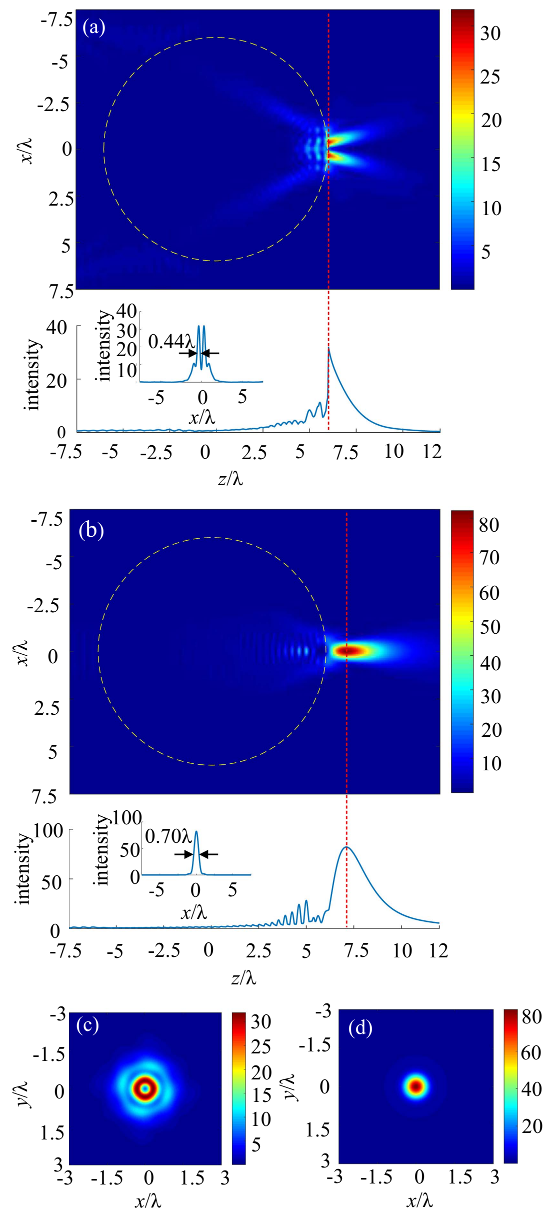

Fig. 2. Electric field intensity distribution $|E|^2$ of the PNJ generated by a dielectric sphere ($R = \lambda$) under illumination by left circularly polarized Laguerre–Gaussian beams with topological charges (a) $m = 2$ and (b) $m = 0$. For each case, the top plot is the $|E|^2$ of the PNJ, while the bottom one is the longitudinal intensity profile. The inset is the transverse profile with marked full width at half-maximum, corresponding to the dashed red line that crosses the maximum intensity point of the PNJ. (c) and (d) plot $|E|^2$ at the focal planes of the PNJs in (a) and (b), respectively.

by selecting the appropriate optical materials. Figure 3(c) illustrates the dependence of P_z on the topological charge m of the incident LG beam, showing that a flexible P_z distribution can be obtained by tuning the optical vortex. For example, when the LCP vortex beam has $m = 2$, the P_z of the generated PNJ has moderate forward energy flow at the hollow ring but the largest

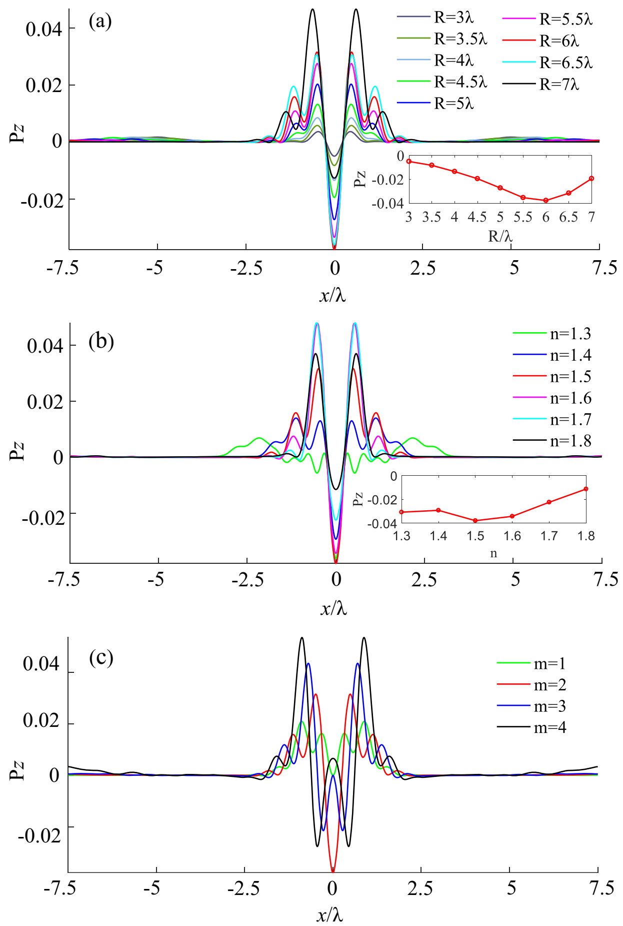

Fig. 3. Longitudinal energy flow P_z at the focal plane of the PNJs generated by left circularly polarized Laguerre–Gaussian beams with (a) fixed topological charge $m = 2$ and refractive index $n = 1.5$ but different microsphere radii R; (b) fixed $m = 2$, $R = 6\lambda$ but different n; and (c) fixed $n = 1.5$, $R = 6\lambda$ but different m. Insets: P_z at $x = 6$.

reverse energy flow along the optical axis among all cases in Fig. 3(c).

To understand better the reverse P_z of the proposed donut-like PNJ, we numerically study the energy-flow distribution in the tangential plane, shown in Fig. 4. For both donut-like and conventional PNJs, the energy flow of the incident light beam is deflected by the dielectric microsphere and then converges; however, in the former case, the hollow-ring-distributed LCP-LG beam with $m = 2$ yields a tube-like divergence after the focusing process of the PNJ: a hollow center where reverse energy flow appears and forms in the focal field.

So far, our investigation of the reverse energy flow in the donut-like PNJ has been numerical, but a more analytical approach is also possible and preferable. PNJ generation can be viewed as analogous to the tight-focusing process of a high NA lens, which can also exhibit reverse energy flow when the incident light is a circularly polarized vortex beam[27,28]. The electromagnetic field of a sharply focused LCP vortex beam can be found theoretically from the RW formulas[29]:

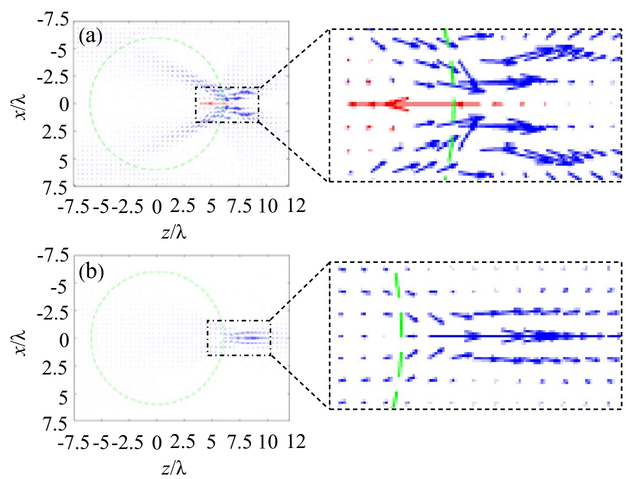

Fig. 4. Energy flow of the PNJs generated by a dielectric sphere ($R = 6\lambda$, $n = 1.5$) illuminated by left circularly polarized Laguerre–Gaussian beams with topological charges (a) $m = 2$ and (b) $m = 0$, corresponding to Figs. 2(a) and 2(b), respectively. The blue arrows depict the forward energy flow, and the red arrows depict the reverse flow.

$$\begin{aligned}
E_x &= -\frac{ikf}{2}\int_0^{\alpha}\sqrt{\cos\theta}\sin\theta e^{ikz\cos\theta}A_m(\theta)\\
&\quad\times[(\cos\theta-1)i^{m-2}J_{m-2}(kr\sin\theta)e^{i(m-2)\phi}\\
&\quad+(1+\cos\theta)i^mJ_m(kr\sin\theta)e^{im\phi}]\mathrm{d}\theta,\\
E_y &= -\frac{ikf}{2}\int_0^{\alpha}\sqrt{\cos\theta}\sin\theta e^{ikz\cos\theta}A_m(\theta)\\
&\quad\times[i(\cos\theta-1)i^{m-2}J_{m-2}(kr\sin\theta)e^{i(m-2)\phi}\\
&\quad-i(1+\cos\theta)i^mJ_m(kr\sin\theta)e^{im\phi}]\mathrm{d}\theta,\\
H_x &= -\frac{ikf}{2c}\int_0^{\alpha}\sqrt{\cos\theta}\sin\theta e^{ikz\cos\theta}A_m(\theta)\\
&\quad\times[i(\cos\theta-1)i^{m-2}J_{m-2}(kr\sin\theta)e^{i(m-2)\phi}\\
&\quad+i(1+\cos\theta)i^mJ_m(kr\sin\theta)e^{im\phi}]\mathrm{d}\theta,\\
H_y &= -\frac{ikf}{2c}\int_0^{\alpha}\sqrt{\cos\theta}\sin\theta e^{ikz\cos\theta}A_m(\theta)\\
&\quad\times[(1-\cos\theta)i^{m-2}J_{m-2}(kr\sin\theta)e^{i(m-2)\phi}\\
&\quad+(1+\cos\theta)i^mJ_m(kr\sin\theta)e^{im\phi}]\mathrm{d}\theta,
\end{aligned}\tag{2}$$

where

$$A_m(\theta)=\left(\frac{\sqrt{2}f\sin\theta}{\omega}\right)^{|m|}\exp\left(-\frac{f^2\sin^2\theta}{\omega^2}\right),\tag{3}$$

$J_m(\cdot)$ is the Bessel function, $\alpha = \arcsin(\mathrm{NA})$, f is the focal length, k is the wave vector, and m is the topological charge.

The longitudinal component of the Poynting vector is then

$$P_z=\frac{c}{8\pi}\mathrm{Re}(E_xH_y^*-E_yH_x^*),\tag{4}$$

where c is the speed of light in vacuum, $\mathrm{Re}(\cdot)$ is the real part of the equation, and * refers to the conjugate. Here, we take the

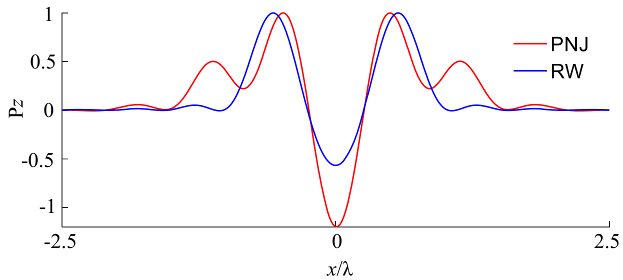

Fig. 5. Longitudinal component of the Poynting vector along the x axis in the focal plane of the proposed donut-like PNJ (red curve) compared to that predicted from the RW integral (blue curve). The incident light is a left circularly polarized Laguerre–Gaussian beam with topological charge $m = 2$. The dielectric microsphere has $R = 6\lambda$ and $n = 1.5$, and the NA of the lens is one.

conventional interpretation of energy flow by using the Poynting vector[30,31], which is numerically confirmed to conservation of energy and is consistent with other researches[27–29].

For the LCP-LG light beam with $m = 2$, the longitudinal component of the Poynting vector of the tight-focusing field from a high NA lens (NA = 1) is calculated and plotted in Fig. 5. Like the Poynting vector of the numerically simulated donut-like PNJ under the same illumination, the analytical P_z appears to be reverse in the vicinity of the hollow center of the focal field. This helps provide an intuitive understanding of the donut-like PNJ. However, the PNJ, as a highly confined propagating beam with a subwavelength beamwidth, has a reverse energy flow of larger magnitude and more degrees of freedom for engineering the donut-like field, thus allowing more flexibility in applications.

3. Conclusion

In conclusion, we propose and investigate a novel donut-like PNJ formed by illuminating a dielectric microsphere with a circularly polarized vortex beam. We numerically study the dependence of PNJ properties on the vortex topological charge and the geometry and refractive index of the microsphere, demonstrating the subwavelength hollow-ring shape of the PNJ field and the existence of longitudinal reverse energy flow at the focal plane. In addition, we explain this unique PNJ property by an approximation of the tight-focusing process, analytically modeled with the RW vector-diffraction integral. The donut-like PNJ, with its structured focal field and unusual energy-flow distribution, may be applicable to novel optical trapping and micromanipulation.

Acknowledgement

This work was supported by the National Key R&D Program of China (Nos. 2018YFA0306200 and 2017YFA0303700), the National Natural Science Foundation of China (NSFC) (Nos. 91750202, 61805119, 61604073, and 11404170), the Natural Science Foundation of Jiangsu Province of China (Nos. BK20160839 and BK20180469), and the Scientific Research Project of Nanjing University of Posts and Telecommunications (No. NY219045).

References

1. Z. Chen, A. Taflove, and V. Backman, "Photonic nanojet enhancement of backscattering of light by nanoparticles: a potential novel visible-light ultramicroscopy technique," Opt. Express **12**, 1214 (2004).
2. Z. B. Wang, W. Guo, L. Li, B. Luk'yanchuk, A. Khan, Z. Liu, Z. C. Chen, and M. H. Hong, "Optical virtual imaging at 50 nm lateral resolution with a white-light nanoscope," Nat. Commun. **2**, 218 (2011).
3. A. Darafsheh, C. Guardiola, A. Palovcak, J. C. Finlay, and A. Carabe, "Optical super-resolution imaging by high-index microspheres embedded in elastomers," Opt. Lett. **40**, 5 (2015).
4. G. Huszka, H. Yang, and M. A. M. Gijs, "Microsphere-based super-resolution scanning optical microscope," Opt. Express **25**, 15079 (2017).
5. D. Gerard, J. Wenger, A. Devilez, D. Gachet, B. Stout, N. Bonod, E. Popov, and H. Rigneault, "Strong electromagnetic confinement near dielectric microspheres to enhance single-molecule fluorescence," Opt. Express **16**, 15297 (2008).
6. P. K. Upputuri and M. Pramanik, "Microsphere-aided optical microscopy and its applications for super-resolution imaging," Opt. Commun. **404**, 32 (2017).
7. F. Wang, S. Yang, H. Ma, P. Shen, N. Wei, M. Wang, Y. Xia, Y. Deng, and Y.-H. Ye, "Microsphere-assisted super-resolution imaging with enlarged numerical aperture by semi-immersion," Appl. Phys. Lett. **112**, 023101 (2018).
8. E. McLeod and C. B. Arnold, "Subwavelength direct-write nanopatterning using optically trapped microspheres," Nat. Nanotech. **3**, 413 (2008).
9. A. Jacassi, F. Tantussi, M. Dipalo, C. Biagini, N. Maccaferri, A. Bozzola, and F. De Angelis, "Scanning probe photonic nanojet lithography," ACS Appl. Mater. Interfaces **9**, 32386 (2017).
10. Y. C. Li, H. B. Xin, H. X. Lei, L. L. Liu, Y. Z. Li, Y. Zhang, and B. J. Li, "Manipulation and detection of single nanoparticles and biomolecules by a photonic nanojet," Light: Sci. Appl. **5**, e16176 (2016).
11. A. Shakhov, A. Astafiev, and V. Nadtochenko, "Microparticle manipulation using femtosecond photonic nanojet-assisted laser cavitation," Opt. Lett. **43**, 1858 (2018).
12. Y. C. Li, H. B. Xin, X. S. Liu, Y. Zhang, H. X. Lei, and B. J. Li, "Trapping and detection of nanoparticles and cells using a parallel photonic nanojet array," ACS Nano **10**, 5800 (2016).
13. S. C. Kong, A. V. Sahakian, A. Taflove, and V. Backman, "Photonic nanojet-enabled optical data storage," Opt. Express **16**, 13713 (2008).
14. S. C. Kong, A. V. Sahakian, A. Heifetz, A. Taflove, and V. Backman, "Robust detection of deeply subwavelength pits in simulated optical data-storage disks using photonic jets," Appl. Phys. Lett. **92**, 211102 (2008).
15. A. Heifetz, S. Kong, A. V. Sahakian, A. Taflove, and V. Backman, "Photonic nanojets," J. Comput. Theoretical Nanos. **6**, 1979 (2009).
16. B. S. Luk'yanchuk, R. Paniagua-Domínguez, I. Minin, O. Minin, and Z. Wang, "Refractive index less than two: photonic nanojets yesterday, today and tomorrow," Opt. Mater. Express **7**, 1820 (2017).
17. Y. C. Shen, L. H. V. Wang, and J. T. Shen, "Ultralong photonic nanojet formed by a two-layer dielectric microsphere," Opt. Lett. **39**, 4120 (2014).
18. G. Q. Gu, R. Zhou, Z. C. Chen, H. Y. Xu, G. X. Gai, Z. P. Gai, and M. H. Hong, "Super-long photonic nanojet generated from liquid-filled hollow microcylinder," Opt. Lett. **40**, 625 (2015).
19. B. F. Zhang, J. J. Hao, Z. Shen, H. Wu, K. Zhu, J. Xu, and J. P. Ding, "Ultralong photonic nanojet formed by dielectric microtoroid structure," Appl. Opt. **57**, 8331 (2018).
20. L. Y. Yue, O. V. Minin, Z. B. Wang, J. N. Monks, A. S. Shalin, and I. V. Minin, "Photonic hook: a new curved light beam," Opt. Lett. **43**, 771 (2018).
21. S. Zhou, "Twin phonotic hooks generated from two coherent illuminations of a micro-cylinder," J. Opt. **22**, 085602 (2020).

22. I. V. Minin, O. V. Minin, G. M. Katyba, N. V. Chernomyrdin, V. N. Kurlov, K. I. Zaytsev, L. Yue, Z. Wang, and D. N. Christodoulides, "Experimental observation of a photonic hook," Appl. Phys. Lett. **114**, 031105 (2019).
23. H. Guo, Y. Han, X. Weng, Y. Zhao, G. Sui, Y. Wang, and S. Zhuang, "Near-field focusing of the dielectric microsphere with wavelength scale radius," Opt. Express, **21**, 2434 (2013).
24. T. Zeng and J. Ding, "Three-dimensional multiple optical cages formed by focusing double-ring shaped radially and azimuthally polarized beams," Chin. Opt. Lett. **16**, 031405 (2018).
25. Z. Gu, X. Wang, J. Wang, F. Fan, and S. Chang, "Sidelobe suppression and axial resolution enhancement in 4pi microscopy with higher-order radially polarized Laguerre–Gaussian beams using subtractive imaging," Chin. Opt. Lett. **17**, 121103 (2019).
26. J. Wang, X. Wang, and M. Zeng, "Broadband transverse displacement sensing of silicon hollow nanodisk under focused radial polarization illumination in the near-infrared region," Chin. Opt. Lett. **18**, 063602 (2020).
27. V. V. Kotlyar, A. A. Kovalev, and A. G. Nalamov, "Energy density and energy flux in the focus of an optical vortex: reverse flux of light energy," Opt. Lett. **43**, 2921 (2018).
28. V. V. Kotlyar, A. G. Nalimov, and A. A. Kotlyar, "Helical reverse flux of light of a focused optical vortex," J. Opt. **20**, 095603 (2018).
29. B. Richards and E. Wolf, "Electromagnetic diffraction in optical systems, II. Structure of the image field in an aplanatic system," Proc. R. Soc. A **253**, 358 (1959).
30. M. Born and E. Wolf, *Principles of Optics*, 7th ed. (Cambridge University, 1999).
31. M. V. Berry, "Optical currents," J. Opt. A **11**, 094001 (2009).